NANO LETTERS

Letter

pubs.acs.org/NanoLett

Strong Enhancement of Second Harmonic Emission by Plasmonic Resonances at the Second Harmonic Wavelength

Bernd Metzger,* Lili Gui, Jaco Fuchs, Dominik Floess, Mario Hentschel, and Harald Giessen

4th Physics Institute and Research Center SCoPE, University of Stuttgart, Pfaffenwaldring 57, 70569 Stuttgart, Germany

Supporting Information

ABSTRACT: We perform second harmonic spectroscopy of aluminum nanoantenna arrays that exhibit plasmonic resonances at the second harmonic wavelength between 450 and 570 nm by focusing sub-30 fs laser pulses tunable from 900 to 1140 nm onto the nanoantenna arrays. We find that *a plasmonic resonance at the second harmonic wavelength* boosts the overall nonlinear process by more than an order of magnitude. In particular, in the measurement the resonant second harmonic polarization component is a factor of about 70 stronger when compared to the perpendicular off-resonant second harmonic polarization. Furthermore, the maximum of the second harmonic conversion efficiency is found to be slightly blue-shifted with respect to the peak of the linear optical far-field spectrum. This fact can be understood from a simple model that accounts for the almost off-resonant absorption at the fundamental wavelength and the resonant emission process at the second harmonic.

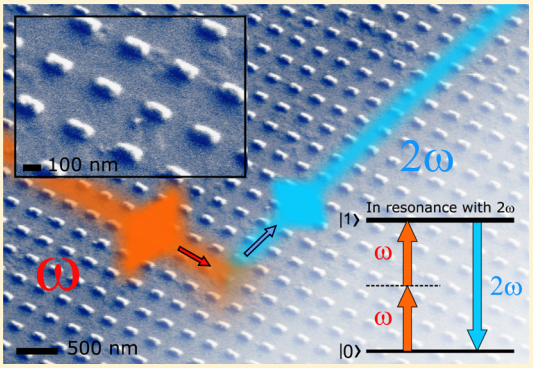

KEYWORDS: *Nanooptics, plasmonics, nonlinear optics, spectroscopy, second harmonic generation*

Resonant plasmonic nanostructures are key for enhancing optical nonlinearities at the nanoscale.[1] Their ability to channel far-field radiation to subwavelength dimensions and vice versa renders them highly attractive to boost nonlinear optical effects.[2,3] In general, two main configurations for the enhancement come to mind: First, a plasmonic nanoantenna is in resonance to the incoming radiation and hence, the field enhancement effect of the fundamental field amplifies the nonlinear conversion. Second, the generated nonlinear signal is efficiently radiated to the far-field by a plasmonic nanoantenna that is resonant to the local nonlinear field.[4,5] So far, the first configuration has been investigated for the enhancement of second harmonic[6−12] (SH) or third harmonic generation,[13−19] nonlinear four wave mixing,[20,21] and optical rectification.[22] Furthermore, in very recent publications the authors combined both configurations, by designing complex plasmonic nanostructures that are resonant to the fundamental *and* the nonlinear field,[23−28] referred to as double resonant antennas. These nanostructures allowed for observation of extraordinary high conversion efficiencies in nonlinear optical experiments. However, in these studies it is hard to disentangle the just mentioned contributions to the nonlinear signal enhancement, particularly, the field enhancement at the fundamental wavelength and potentially the enhanced emission at the frequency of the nonlinear signal.

In this Letter, we address exactly this issue. We investigate the SH response of aluminum rod-type nanoantenna arrays that are solely in resonance with the SH signal. Although noncentrosymmetric plasmonic nanostructures are commonly believed to exhibit a higher SH conversion efficiency, such structures also would show higher order plasmonic modes which subsequently render it more complicated to disentangle the different contributions to the nonlinear signal enhancement. Hence, rod-type plasmonic nanoantennas, which despite their symmetry properties have been found to feature a distinct SH response, probably due to surface irregularities,[12,29−31] allow us to unravel the SH enhancement that can be achieved by a plasmonic mode that resonantly radiates the generated SH light to the far-field. In particular, we find that the SH polarization radiated by the plasmonic mode of the antennas is resonantly enhanced by more than an order of magnitude when compared to the perpendicularly polarized SH signal that does not couple to the plasmonic mode for emission enhancement. Furthermore, the maximum SH conversion efficiency is found to be slightly blue-shifted with respect to the peak of the linear optical reflectance spectrum. This behavior can be explained by a model that accounts for the almost off-resonant absorption at frequency ω and the resonant emission process at 2ω.

To experimentally investigate the emission enhancement by plasmonic nanoantennas for SH generation, we fabricated aluminum nanoantenna arrays with an area of 100 × 100 μm^2 on a fused silica substrate using standard electron beam lithography. In contrast to gold, which is hampered by interband absorptions in the visible spectral range,[32] aluminum nanostructures can exhibit well-modulated plasmonic modes in the SH wavelength range between 450 and 570 nm;[33] small

Received: February 24, 2015
Revised: April 13, 2015
Published: April 13, 2015

DOI: 10.1021/acs.nanolett.5b00747
Nano Lett. 2015, 15, 3917−3922

interband absorption effects are only seen around 800 nm.[34] The height and width of the individual rod-type nanoantennas are 50 and 60 nm, respectively, and their length is varied from 120 to 150 nm. The lattice constant in both directions is 300 nm.

Before performing SH spectroscopy experiments, we measured the reflectance spectra of the nanoantenna arrays under normal incidence using a linearly p- or s-polarized white light source. Beyond their common meaning in our manuscript, p- and s-polarization denote the polarization direction parallel and perpendicular to the nanoantenna long axis, respectively. For the reference reflection we utilized a 100 nm thick aluminum film. In Figure 1a an exemplary reflectance spectrum

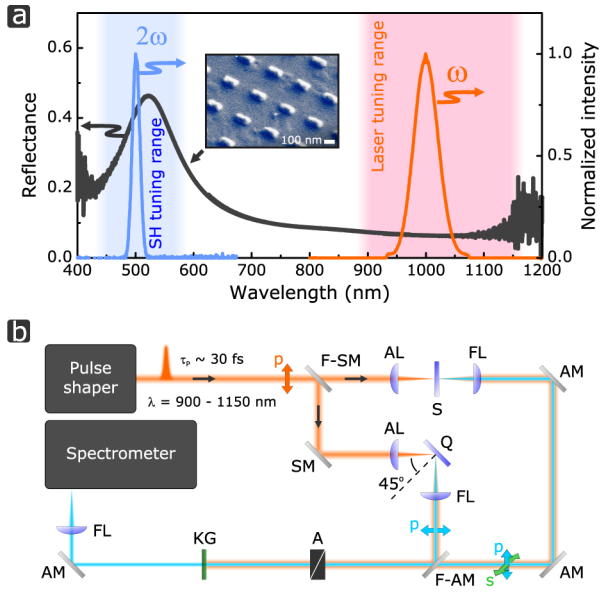

Figure 1. (a) Exemplary measured laser spectrum (red) and its corresponding measured SH spectrum (blue) with respect to the measured reflectance spectrum of an aluminum nanoantenna array (black). The inset shows a tilted scanning electron micrograph of the corresponding nanoantenna array. (b) Experimental setup for measuring polarization-resolved SH spectra. F: flip mirror, SM: silver mirror, AM: aluminum mirror, AL: aspheric lens, FL: fused silica lens, S: sample, Q: quartz crystal, A: analyzer, KG: KG filters.

(black) measured in p-polarization of a nanoantenna array is shown, which exhibits a longitudinal localized surface plasmon resonance at a central wavelength of about 520 nm. The measured s-polarized reflectance spectra exhibit no distinct features in the considered spectral range and can be found in the Supporting Information.

The nonlinear optical properties of resonant plasmonic nanostructures usually exhibit strong frequency dependencies. To determine the spectral position of highest conversion efficiency, it is therefore crucial to utilize a tunable laser source so that a nonlinear spectrum can be recorded.[8,9,17,35] Hence, we utilize sub-30 fs laser pulses from an amplitude and phase adjustable pulse shaper,[36] which are tunable in the spectral range from 900 to 1140 nm with an average power of about 20 mW. In Figure 1a an exemplary measured laser spectrum (red) at a central wavelength of 1000 nm and a corresponding measured SH spectrum (blue) at a wavelength of 500 nm are displayed. The red and the blue shaded areas indicate the tuning range of the central wavelength of our laser source and the SH signals, respectively.

A schematic illustration of our experimental setup for SH spectroscopy is depicted in Figure 1b. Using a flip mirror the p-polarized laser pulses from the pulse shaper either can be focused onto the sample under normal incidence or onto a birefringent quartz crystal under an angle of incidence of 45°, where a reference SH signal can be generated. By normalizing the SH spectroscopy measurements to this reference SH we account for slightly different laser pulse parameters and possible wavelength dependencies of the optical components in our setup when tuning the fundamental laser wavelength.[8] Furthermore, the laser pulses are focused by identical 75 mm focal length achromatic lenses leading to a spot size in the focus of about 50 μm. The SH signals radiated in forward direction from the nanoantenna arrays and the SH signals reflected from the quartz crystal surface are recollimated using a fused silica lens. Subsequently, the two beam paths are recombined, sent through an analyzer, and separated from the fundamental laser light by a series of Schott KG filters. Finally, the SH signals are measured using a Peltier-cooled CCD camera attached to a spectrometer.

Following to the SH spectroscopy experiments, we spectrally integrate the measured SH signals to obtain a scalar value that represents the corresponging SH intensity. Finally, the polarization-resolved SH intensity data points are normalized to the reference SH signals from the quartz crystal and plotted as a function of the SH wavelength together with the reflectance spectrum of the corresponding nanoantenna array.

The experimental results are shown in Figure 2a for various nanoantenna arrays with different nanoantenna lengths l increasing from top to bottom. A number of important observations can be made: First, for increasing antenna length l the localized surface plasmon resonances red-shift as expected from the linear reflectance spectra (black). Second, together with the red-shift, the linewidth of the plasmon resonances increases monotonically, which most likely can be attributed to an increased coupling between the different antenna elements in an entire nanoantenna array.[9,37] Third, the p-polarized SH signals (blue) almost follow the reflectance spectra of the nanoantenna arrays; however, there is an obvious trend for the peaks of the SH intensities to be slightly blue-shifted with respect to the peaks of the linear reflectance spectra. Fourth, we also observe comparably weak s-polarized SH signals (green), increasing toward shorter wavelength.

Obviously, the p-polarized SH signals are resonantly radiated by the plasmonic nanoantennas. We ask now the question how to understand the physical reason for the small but distinct blue-shift of the peak of the p-polarized SH intensities, and moreover, we want to comprehend the origin for the increase of the s-polarized SH signals toward shorter wavelength.

In order to gain more insight into the nonlinear optical processes and to understand the spectral behavior of the SH intensities, we consider the polarizability $\alpha(\omega)$ of a single nanoantenna. For metal nanostructures that exhibit a single plasmonic mode the spectral dependency of the polarizability can be approximated by a Lorentzian lineshape,[38]

$$\alpha(\omega) = \frac{A}{\omega^2 - \omega_0^2 + 2i\gamma\omega} \quad (1)$$

where ω_0 denotes the resonance frequency, γ the linewidth, i.e., the damping of the plasmonic mode, and A an overall amplitude. In the following the rod-type nanoantenna arrays are treated as a plane of oscillating dipoles. The scattering of a plane of radiating dipoles is proportional to the velocity of the

DOI: 10.1021/acs.nanolett.5b00747
Nano Lett. 2015, 15, 3917−3922

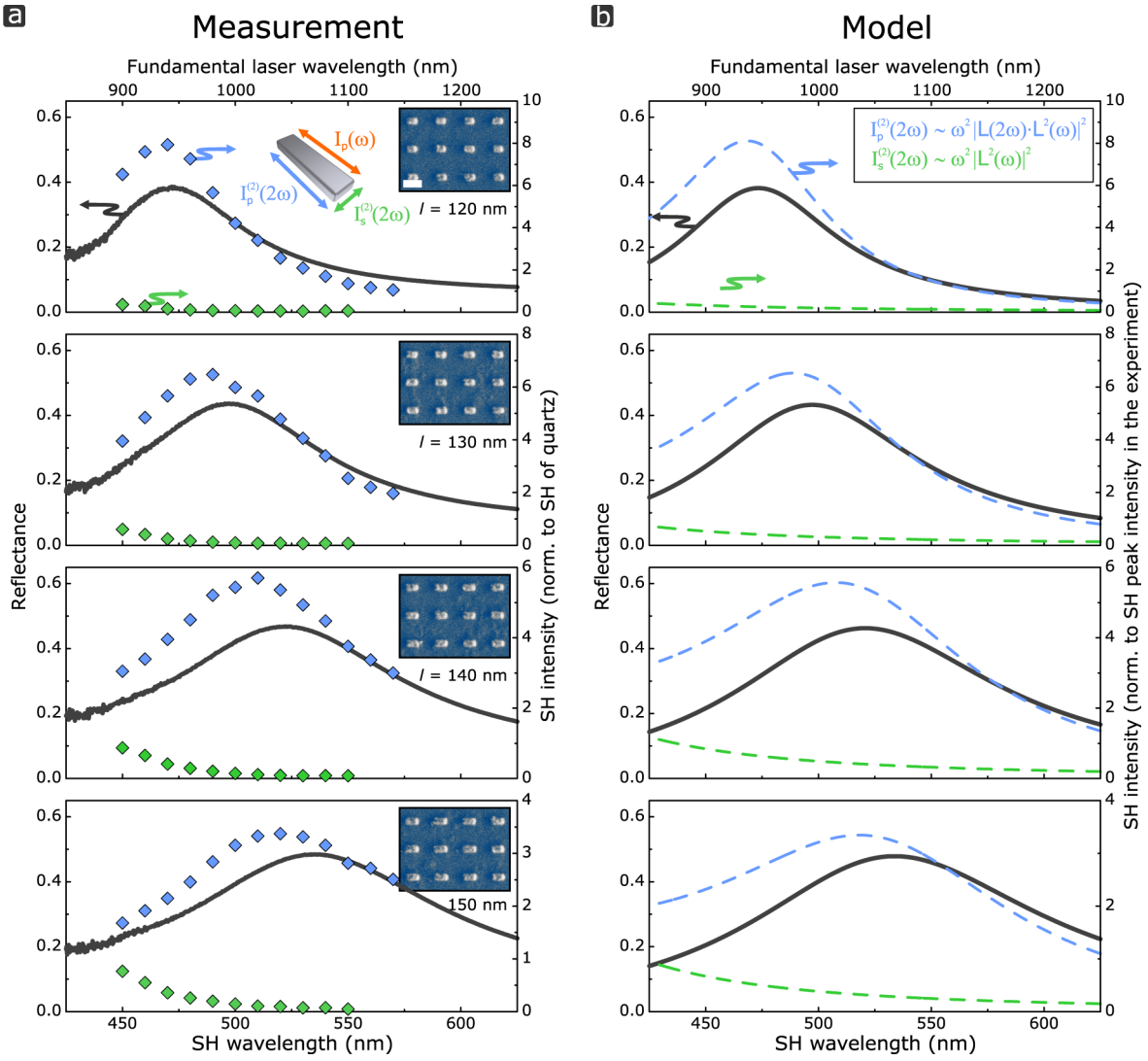

Figure 2. Measured (a) and modeled (b) polarization-resolved SH spectra together with the corresponding reflectance spectra of four aluminum nanoantenna arrays with different nanoantenna length l increasing from top to bottom from about 120 to 150 nm plotted over the SH wavelength. The top axis shows the corresponding fundamental laser wavelength. The insets show corresponding scanning electron micrographs. The scale bar is 200 nm.

oscillating charges,[39] hence we obtain for the scattering spectrum C_{scat}:

$$C_{scat} \propto \omega^2 |\alpha(\omega)|^2 = \frac{A^2\omega^2}{(\omega^2 - \omega_0^2)^2 + 4\gamma^2\omega^2} \quad (2)$$

The scattering spectrum C_{scat} can be used to fit the measured reflectance spectra. The corresponding fitted reflectance spectra are shown in Figure 2(b, black).

To describe the SH response of the aluminum nanoantenna arrays, we introduce the phenomenological field enhancement factor $L(\omega)$,[38] which accounts for the local field enhancement at the fundamental and the SH field via $E_{loc}(\omega) = L(\omega)E(\omega)$, where $E_{loc}(\omega)$ is the locally enhanced electric field amplitude and $E(\omega)$ the electric far-field amplitude, respectively. Except for a proportionality constant, the field enhancement factor $L(\omega)$ exhibits the same functional behavior as the polarizability $\alpha(\omega)$.[40] Furthermore, due to causality far off resonance, the field enhancement caused by the plasmonic mode has to vanish, and hence we normalize $L(\omega)$ so that its value at zero frequency is equal to one ($L(\omega = 0) = 1$).

As a reminder, in the experiment the p-polarized SH signals are resonantly emitted by the plasmonic mode, whereas the s-polarized SH signals are not. Therefore, the field enhancement factor $L(2\omega)$ only enters into the p-polarized component. Hence, the s- and p-polarized second order nonlinear polarizations $P_{s,p}^{(2)}(\omega)$ take the following form:[38]

$$P_p^{(2)}(2\omega) \propto L(2\omega)\, \chi_{ppp}^{(2)}\, L^2(\omega)\, E_p^2(\omega) \quad (3)$$

$$P_s^{(2)}(2\omega) \propto \chi_{spp}^{(2)}\, L^2(\omega)\, E_p^2(\omega) \quad (4)$$

where $\chi_{spp}^{(2)}$ and $\chi_{ppp}^{(2)}$ correspond to effective second-order susceptibilities describing the overall efficiency of an aluminum nanoantenna element without field enhancement, to convert two p-polarized photons into an s- or a p-polarized photon at twice the frequency, respectively.

For simplicity, we assume in the following the absolute values of $\chi_{spp}^{(2)}$ and $\chi_{ppp}^{(2)}$ to be equal. At first sight it might appear unexpected that the values of the effective SH tensor elements are similar in magnitude. However, when comparing the model

DOI: 10.1021/acs.nanolett.5b00747
Nano Lett. 2015, 15, 3917−3922

to the experiment further below it turns out to be a good approximation.

Finally, the emitted s- and p-polarized SH intensities $I_{s,p}^{(2)}$ are obtained by describing the nanoantenna arrays as planes of radiating dipoles oscillating at the SH frequency:[39]

$$I_p^{(2)}(2\omega) \propto \omega^2 |L(2\omega)\cdot L^2(\omega)|^2 \quad (5)$$

$$I_s^{(2)}(2\omega) \propto \omega^2 |L^2(\omega)|^2 \quad (6)$$

The modeled s- and p-polarized SH intensities are depicted in Figure 2b together with the corresponding fitted linear reflectance spectra. First of all, the enhanced radiation efficiency of the p-polarized SH intensity (blue) is well described by our model, as is the slight blue-shift of its peak position. Moreover, also the increase of the s-polarized SH intensity (green) toward shorter wavelength is confirmed. Admittedly, the relative SH signal strength between the four nanoantenna arrays is not described in a complete fashion by our simple model. In the measurement the p-polarized SH intensities are found to increase toward shorter nanoantenna length, which most likely can be attributed to the previously mentioned narrowing of the resonance linewidth of the plasmon resonances.[9] This trend also qualitatively can be confirmed and understood by the field enhancement factors, which increase in amplitude for decreasing resonance linewidth. However, the quantitative agreement of the relative SH intensities of the four nanoantenna arrays between the measurement and the model is limited. Therefore, the modeled p-polarized SH intensities have been independently scaled so that the modeled peak values agree with the measured SH peak value of the corresponding nanoantenna array. However, the relative SH signal strengths between the two SH polarization components of one and the same nanoantenna array are well-approximated by our model, since the s- and p-polarized SH intensities have been scaled with the same factor, respectively. This also demonstrates that the above assumption of at least similar second-order susceptibilities was justified.

The results of the modeling also allow us to understand the details of the SH spectra: Although the nanoantenna arrays are resonant to the SH wavelength, the tails of the resonances reach up to the fundamental laser wavelength. Hence, the absorbance of the fundamental laser light is increased when the laser is tuned toward shorter wavelength, which leads to the increase of the s-polarized SH intensity. Furthermore, the blue-shift of the p-polarized SH intensity is closely related to this phenomenon. The radiation efficiency for the p-polarized SH signals peaks at the far-field resonance frequency ω_0; however, due to the increased absorption for the incoming laser radiation tuned toward shorter wavelengths, the overall SH intensity curve shifts to the blue.

Intuitively, this blue-shift is more pronounced as the damping of the plasmon resonances increases. A broader linewidth leads to a longer tail of the plasmon resonances and therefore to a higher influence at the fundamental laser wavelength. In order to capture the blue-shift quantitatively, we extracted the peak positions of the p-polarized SH intensities from the measurement and the model for the four investigated nanoantenna arrays of Figure 2 and plotted the measured blue-shift with respect to the modeled blue-shift in Figure 3. Since the linewidth of the plasmon resonances becomes broader for increasing antenna length l, the blue-shift increases as well, as expected from our explanation.

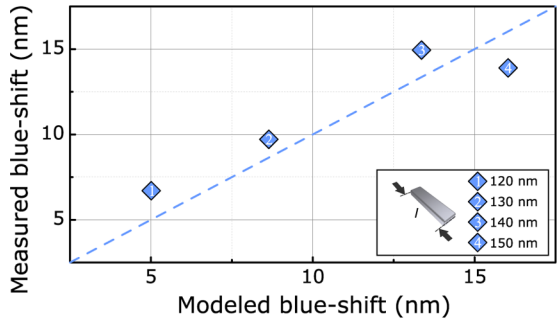

Figure 3. Measured blue-shift of the peak of the p-polarized SH conversion efficiencies with respect to the blue-shift extracted from the model, for the four nanoantenna arrays depicted in Figure 2.

Finally, the measurements and the model allow us to approximate the SH emission enhancement by the plasmonic resonances at the SH wavelength. Therefore, we consider the p-polarized SH intensity divided by the s-polarized SH intensity. Both are influenced by the field enhancement factor $L(\omega)$ in the absorption process at the fundamental wavelength; however, only the p-polarized component is boosted by the field enhancement factor $L(2\omega)$ at the SH frequency. Hence, by dividing the p- and s-polarized SH intensities, we eliminate the absorbance process and are able to extract the emission enhancement for SH generation. In the model the ratio of the p- and s-polarized SH intensities are given by

$$\frac{I_p^{(2)}(2\omega)}{I_s^{(2)}(2\omega)} \propto |L(2\omega)|^2 \quad (7)$$

For the nanoantenna array with an antenna length of 130 nm, the result of these considerations is depicted in Figure 4. In the measurement and the model, we observe a peak ratio between the two SH polarization components well above an order of magnitude and with a maximum value in the measurement of about 70. Most interestingly, we find the peak of the SH emission enhancement red-shifted with respect to the peak of the far-field reflectance spectrum. The origin of this red-shift is the difference between spectral peak positions of plasmonic near-field and far-field quantities[17,41−44] and is caused by the damping of the plasmonic mode.

In the measurement and the model, we observe a slightly different absolute value in the ratio of the p- and s-polarized SH intensity. Primarily this difference shows that our assumption of equal second-order susceptibilities was only a rough estimate. Hence, in the experiment the peak ratio of about 70 partially can be attributed to a slightly smaller value of $\chi_{spp}^{(2)}$ when compared to $\chi_{ppp}^{(2)}$, while the larger part stems from the enhanced emission by the plasmonic resonance located at the SH wavelength, described by the field enhancement factor $L(2\omega)$ displayed in Figure 4b. Furthermore, we utilized a highly simplified model to describe the SH response of the nanoantenna arrays. A precise quantitative analysis might only be achieved using nonlinear electrodynamic scattering theory, also taking the geometry of the nanoantennas and the in- and outgoing partial waves into account.[45] Although our model is not able to capture the SH response of the plasmonic nanoantenna arrays quantitatively, the physical mechanisms and the order of magnitude of the processes can be well understood and described by our simple model.

To summarize, we investigated the enhancement for SH generation by plasmonic nanoantennas that are resonant to the

DOI: 10.1021/acs.nanolett.5b00747
Nano Lett. 2015, 15, 3917−3922

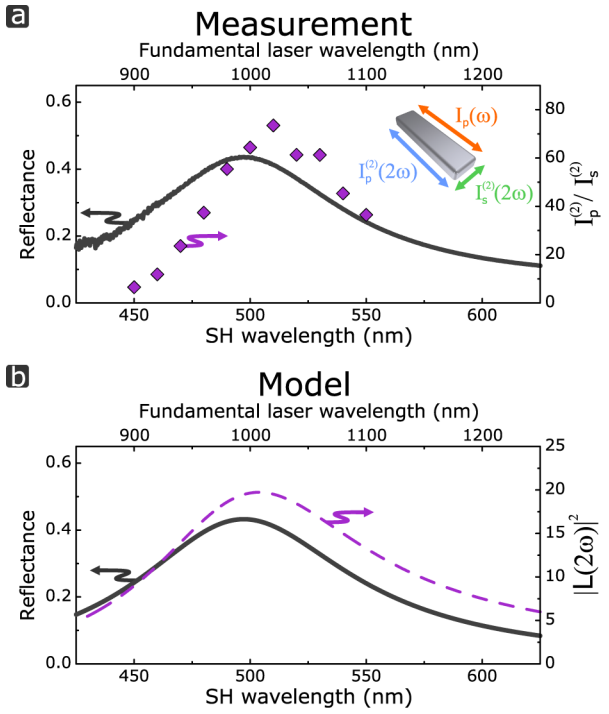

Figure 4. (a) Measured p-polarized SH intensity divided by the s-polarized SH intensity for the nanoantenna array with an antenna length of 130 nm. (b) Absolute value squared of the modeled field enhancement factor $|L(2\omega)|^2$ of the same nanoantenna array as shown in (a) plotted over the SH wavelength. For comparison in both cases also the linear reflectance spectrum (black) of this nanoantenna array is shown.

SH wavelength. We found that the SH polarization component that is boosted by the plasmonic mode is enhanced by more than an order of magnitude when compared to the other SH polarization component. Furthermore, the overall SH conversion efficiency for SH resonant antennas is found to be slightly blue-shifted with respect to the linear optical reflectance spectra. This blue-shift can be explained by a model that accounts for the almost off-resonant absorption at the fundamental wavelength and the resonant emission process at the second harmonic wavelength. Our findings extend the understanding of nonlinear optical processes in plasmonic nanostructures and hence pave the way toward further enhanced nanoscale nonlinearities and nonlinear plasmonic applications.

■ ASSOCIATED CONTENT

Ⓢ Supporting Information

Figure S1, measured s-polarized reflectance spectra of the four aluminum nanoantenna arrays. The Supporting Information is available free of charge on the ACS Publications website at DOI: 10.1021/acs.nanolett.5b00747.

■ AUTHOR INFORMATION

Corresponding Author

*E-mail: b.metzger@physik.uni-stuttgart.de.

Author Contributions

B.M. and L.G. contributed equally to this work.

Notes

The authors declare no competing financial interest.

■ ACKNOWLEDGMENTS

We gratefully acknowledge financial support from the Baden-Württemberg Stiftung (Kompetenznetz Funktionelle Nanostrukturen), from the DFG (SPP1391, ultrafast nanooptics), from the BMBF (13N10146), and the ERC (Complexplas). The authors thank Daniel Drégely for sample fabrication in an early stage of the experiment, Maxim Nesterov for preliminary simulations and Ramon Walter for the evaporation of aluminum.

■ REFERENCES

(1) Kauranen, M.; Zayats, A. V. *Nat. Photonics* **2012**, *6*, 737−748.
(2) Novotny, L.; van Hulst, N. *Nat. Photonics* **2011**, *5*, 83−90.
(3) Mühlschlegel, P.; Eisler, H.-J.; Martin, O. J. F.; Hecht, B.; Pohl, D. W. *Science* **2005**, *308*, 1607−1609.
(4) Wokaun, A.; Bergman, J. G.; Heritage, J. P.; Glass, A. M.; Liao, P. F.; Olson, D. H. *Phys. Rev. B* **1981**, *24*, 849−856.
(5) Moran, A. M.; Sung, J.; Hicks, E. M.; Van Duyne, R. P.; Spears, K. G. *J. Phys. Chem. B* **2005**, *109*, 4501−4506.
(6) Klein, M. W.; Enkrich, C.; Wegener, M.; Linden, S. *Science* **2006**, *313*, 502−504.
(7) Chen, K.; Durak, C.; Heflin, J. R.; Robinson, H. D. *Nano Lett.* **2007**, *7*, 254−258.
(8) Niesler, F. B. P.; Feth, N.; Linden, S.; Wegener, M. *Opt. Lett.* **2011**, *36*, 1533−1535.
(9) Linden, S.; Niesler, F. B. P.; Förstner, J.; Grynko, Y.; Meier, T.; Wegener, M. *Phys. Rev. Lett.* **2012**, *109*, 1.
(10) Zhang, Y.; Grady, N. K.; Ayala-Orozco, C.; Halas, N. J. *Nano Lett.* **2011**, *11*, 5519−5523.
(11) Czaplicki, R.; Husu, H.; Siikanen, R.; Mäkitalo, J.; Kauranen, M.; Laukkanen, J.; Lehtolahti, J.; Kuittinen, M. *Phys. Rev. Lett.* **2013**, *110*, 1−5.
(12) Accanto, N.; Piatkowski, L.; Renger, J.; van Hulst, N. F. *Nano Lett.* **2014**, *14*, 4078−4082.
(13) Lippitz, M.; van Dijk, M. A.; Orrit, M. *Nano Lett.* **2005**, *5*, 799−802.
(14) Klein, M. W.; Tritschler, T.; Wegener, M.; Linden, S. *Phys. Rev. B* **2005**, *72*, 115113.
(15) Utikal, T.; Zentgraf, T.; Paul, T.; Rockstuhl, C.; Lederer, F.; Lippitz, M.; Giessen, H. *Phys. Rev. Lett.* **2011**, *106*, 133901.
(16) Hentschel, M.; Utikal, T.; Giessen, H.; Lippitz, M. *Nano Lett.* **2012**, *12*, 3778.
(17) Metzger, B.; Hentschel, M.; Lippitz, M.; Giessen, H. *Opt. Lett.* **2012**, *37*, 4741−4743.
(18) Aouani, H.; Rahmani, M.; Navarro-Cía, M.; Maier, S. A. *Nat. Nanotechnol.* **2014**, *9*, 290−294.
(19) Chen, S.; Li, G.; Zeuner, F.; Wong, W. H.; Pun, E. Y. B.; Zentgraf, T.; Cheah, K. W.; Zhang, S. *Phys. Rev. Lett.* **2014**, *113*, 033901.
(20) Danckwerts, M.; Novotny, L. *Phys. Rev. Lett.* **2007**, *98*, 026104.
(21) Harutyunyan, H.; Volpe, G.; Quidant, R.; Novotny, L. *Phys. Rev. Lett.* **2012**, *108*, 217403.
(22) Luo, L.; Chatzakis, I.; Wang, J.; Niesler, F. B. P.; Wegener, M.; Koschny, T.; Soukoulis, C. M. *Nat. Commun.* **2014**, *5*, 3055.
(23) Aouani, H.; Navarro-Cia, M.; Rahmani, M.; Sidiropoulos, T. P. H.; Hong, M.; Oulton, R. F.; Maier, S. A. *Nano Lett.* **2012**, *12*, 4997−5002.
(24) Thyagarajan, K.; Rivier, S.; Lovera, A.; Martin, O. J. *Opt. Express* **2012**, *20*, 12860−12865.
(25) Zhang, Y.; Wen, F.; Zhen, Y.-R.; Nordlander, P.; Halas, N. J. P. *Proc. Natl. Acad. Sci. U.S.A.* **2013**, *110*, 9215−9219.
(26) Thyagarajan, K.; Butet, J.; Martin, O. J. F. *Nano Lett.* **2013**, *2013*, 1847−1851.
(27) Ren, M.-L.; Liu, S.-Y.; Wang, B.-L.; Chen, B.-Q.; Li, J.; Li, Z.-Y. *Opt. Express* **2014**, *22*, 28653−28661.

DOI: 10.1021/acs.nanolett.5b00747
Nano Lett. 2015, 15, 3917−3922

(28) Celebrano, M.; Wu, X.; Baselli, M.; Grobmann, S.; Biagioni, P.; Locatelli, A.; Angelis, C. D.; Cerullo, G.; Osellame, R.; Hecht, B.; Duò, L.; Ciccacci, F.; Finazzi, M. *arXiv*: 1412.0698, **2014**.
(29) van Nieuwstadt, J. A. H.; Sandtke, M.; Harmsen, R. H.; Segerink, F. B.; Prangsma, J. C.; Enoch, S.; Kuipers, L. *Phys. Rev. Lett.* **2006**, *97*, 146102.
(30) Bachelier, G.; Butet, J.; Russier-Antoine, I.; Jonin, C.; Benichou, E.; Brevet, P.-F. *Phys. Rev. B* **2010**, *82*, 235403.
(31) Butet, J.; Thyagarajan, K.; Martin, O. J. F. *Nano Lett.* **2013**, *13*, 1787−1792.
(32) Johnson, P. B.; Christy, R. W. *Phys. Rev. B* **1972**, *6*, 4370−4379.
(33) Knight, M. W.; Liu, L.; Wang, Y.; Brown, L.; Mukherjee, S.; King, N. S.; Everitt, H. O.; Nordlander, P.; Halas, N. J. *Nano Lett.* **2012**, *12*, 6000−6004.
(34) McPeak, K. M.; Jayanti, S. V.; Kress, S. J. P.; Meyer, S.; Iotti, S.; Rossinelli, A.; Norris, D. J. *ACS Photonics* **2015**, *2*, 326−333.
(35) Walsh, G. F.; Dal Negro, L. *Nano Lett.* **2013**, *13*, 3111−3117.
(36) Metzger, B.; Steinmann, A.; Giessen, H. *Opt. Express* **2011**, *19*, 24354−24360.
(37) Decker, M.; Feth, N.; Soukoulis, C. M.; Linden, S.; Wegener, M. *Phys. Rev. B* **2011**, *84*, 085416.
(38) Raschke, M. B.; Berweger, S.; Atkin, J. M. *Plasmonics: Theory and Applications*; Springer: New York, 2014; Chapter Ultrafast and Nonlinear Plasmon Dynamics.
(39) Feynman, R. P.; Leighton, R. B.; Sands, M. *The Feynman Lectures on Physics*, Vol. *1*; Addison-Wesley: Boston, 1977; Chapter 30 Diffraction, Formula 30.19.
(40) Maier, S. A. *Plasmonics: Fundamentals and Applications*; Springer: New York, 2007; Chapter 9, Enhancement of Emissive Processes and Nonlinearities, Formula 9.5.
(41) Zuloaga, J.; Nordlander, P. *Nano Lett.* **2011**, *11*, 1280−1283.
(42) Alonso-González, P.; Albella, P.; Neubrech, F.; Huck, C.; Chen, J.; Golmar, F.; Casanova, F.; Hueso, L. E.; Pucci, A.; Aizpurua, J.; Hillenbrand, R. *Phys. Rev. Lett.* **2013**, *110*, 203902.
(43) Menzel, C.; Hebestreit, E.; Mühlig, S.; Rockstuhl, C.; Burger, S.; Lederer, F.; Pertsch, T. *Opt. Express* **2014**, *22*, 9971−9982.
(44) Vogt, J.; Huck, C.; Neubrech, F.; Toma, A.; Gerbert, D.; Pucci, A. *Phys. Chem. Chem. Phys.* **2015**, DOI: 10.1039/C4CP04851B.
(45) O'Brien, K.; Suchowski, H.; Rho, J.; Salandrino, A.; Kante, B.; Yin, X.; Zhang, X. *Nat. Mater.* **2015**, *14*, 379−383.

DOI: 10.1021/acs.nanolett.5b00747
Nano Lett. 2015, 15, 3917−3922